Feasability study for a full hadrondic reconstruction of B_s^0 mesons with the upgraded ALICE detector

Author:
Hanne HOFFMAN
4122577

Supervisors:
Andre MISCHKE
Alessandro GRELLI

January 18, 2017

Physics Utrecht

EMMEΦ
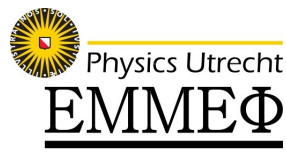
Abstract

This thesis summarizes a simulation study on the feasibility to reconstruct the B_s^0 meson in proton-proton collisions at 14 TeV with the ALICE detector after the upgrade planned in 2018-2019. The decay used for this reconstruction is $B_s^0 \rightarrow D_s^+ D_s^- \rightarrow \phi \pi^+ \phi \pi^- \rightarrow K^+ K^- \phi^+ K^+ K^- \phi^-$. This is a fully hadronic decay, a decay without leptons, which means that all final particles are detectable in the ALICE experiment.

Reconstructing the B_s^0 meson in proton-proton collisions would provide a reference frame for the investigation of the properties of the Quark-Gluon Plasma using the beauty quark as a probe. The Quark Gluon Plasma is a highly energetic state of matter, in which the universe is believed to have existed the first microseconds after the Big Bang.

The conclusion of this study is that it would be recommendable to cut out the low-momentum candidates and the ones with a small distance to the decay vertex of the particle for the reconstruction in order to study the B_s^0 meson through this decay. The rarity and the detectable fraction of the investigated decay combined make that there will not be a sufficient amount of results for reconstruction. Two alternatives are suggested: Using a trigger for decays including a high-energy electron and an alternative reconstruction possibility using a semi-hadronic decay of D_s mesons.

Contents

1 Introduction

1.1 A brief introduction to particle physics

In 1896 Henry Becquerel discovers the phenomenon of radioactivity. Until then, scientists believed that the smallest possible particles where the nuclei and the electrons that form atoms. With Becquerel's discovery that it is possible for a nucleus to transform into another nucleus, the subject of particle physics was born. Since Becquerel's discovery a lot of new particles have been discovered[1].

The currently accepted collection of elementary particles, particles without a substructure, is given by the Standard Model. The Standard Model arranges all elementary particles in three categories: *leptons, quarks* and *bosons*. Figure 1 shows a table with all known elementary particles. The *fermions*, divided in leptons and quarks, are the particles that build up matter. Every fermion has an *antiparticle* with opposite properties. *Bosons* are the force carriers between leptons and quarks that make interactions possible. The *Higgs boson* can be seen as an exited state of the *Higgs field*. The Higgs field is the origin of mass[1][2].

There are three generations of leptons: *electron* (e), *muon* (μ) and *tau* (τ). These three particles all have a corresponding neutrino (ν_e, ν_μ, ν_τ).

There are six types of quarks with all different masses: listed from light to heavy there are *up* (u), *down* (d), *strong* (s), *charm* (c), *beauty* (b) and *top* (t) quarks. The lightest quarks are very common at low temperatures, the heavier quarks are created at high temperatures and decay very fast. The charm, beauty and top quarks are known as the heavy quarks.

The standard model describes three forces: the *weak, strong* and *electromagnetic* force. It does not describe gravity and dark matter interactions. According to the Standard Model, interactions are mediated by *gauge bosons*: the Z, W^+ and W^- boson for the weak force, the gluon for the strong force and the photon for the electromagnetic force. For the different forces, different conservation laws apply, e.g. conservation of charge. An interaction is possible if it follows all conservation laws given by the Standard Model for the participating force[3].

Interactions including one or more leptons are called *semi-leptonic* and *leptonic* interactions. These interactions are always mediated by the weak force.

The currently accepted theory to describe strong interactions is called the theory of *Quantum Chromodynamics* (QCD). This theory assumes all strongly interacting matter, which are gluons and quarks, carries a color: blue, green or red. Quarks are bound in pairs of two (mesons) and three (baryons) hold together by gluons. These are called *hadrons* or *hadronic matter*. Every hadron is color-neutral[1].

Figure 1 – A table of the elementary particles of the Standard Model. Figure adopted from [3].

1.2 The Quark-Gluon Plasma

It is widely believed by physicists that the in the first moments after the Big Bang, matter as we know it had not yet formed. Gluons and quark were in a high energy, fluid-like state, called the Quark-Gluon Plasma (QGP). In this state, the quarks are no longer bound to their color-neutral hadrons, like they are today.

This high energy state of matter is believed to be recreated in high energy heavy-ion collisions, like lead-lead collisions. In Figure 2, the conditions needed for the QGP are shown schematically. To form the QGP either a very high temperature, a very high density, or a combination of these two is needed. At the first, it had such a high temperature that it formed the QGP and than it cooled down due to the expansion and reached a temperature low enough for hadrons to form. In heavy-ion collision experiments ions collide with a speed close to the speed of light they generate so much energy that the temperature rises to a value high enough to create the QGP[4][5].

1.3 High energy probes

The lifetime of the QGP is too short to investigate it directly. A suggested approach to investigate the properties of the QGP is to use heavy flavored quarks
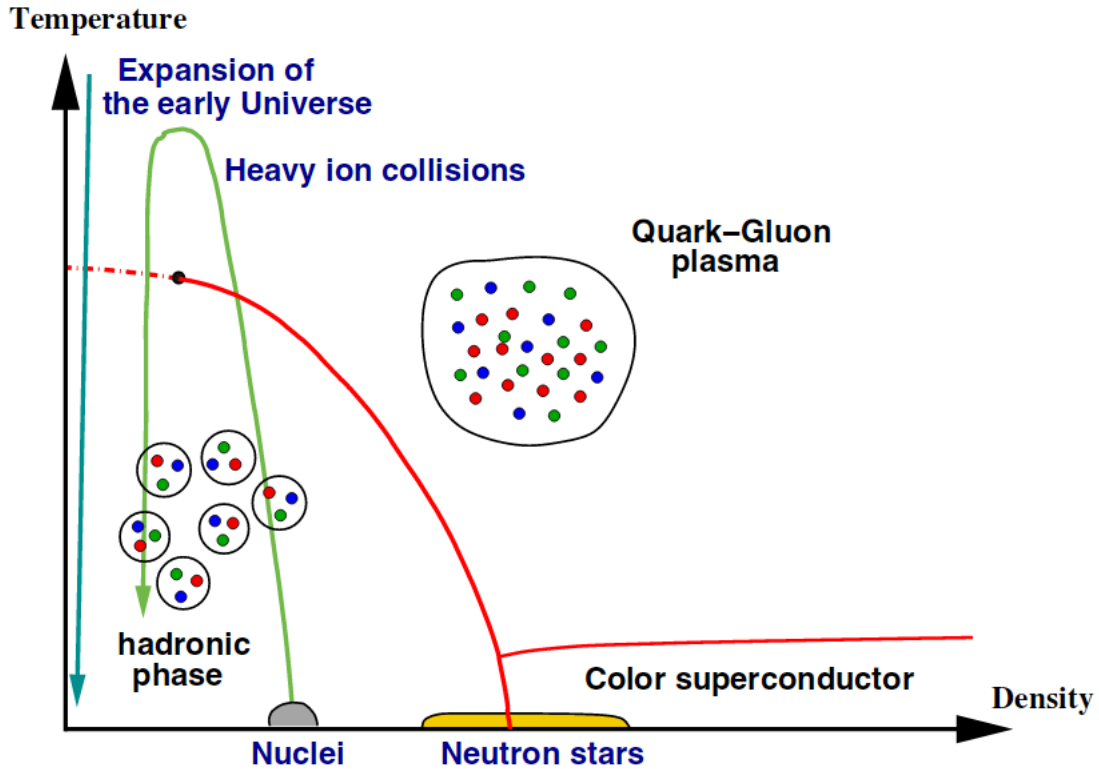
Figure 2 – A schematic representation of a phase-diagram in QCD. The blue arrow represents the expansion of the early universe. The green arrow represents heavy-ion collision experiments. Figure adopted from [6].

(c,b,t) as probes. The energy-loss of a particle passing through can be measured by this method and used to calculate the resistance of the QGP. There are several factors that make heavy quarks suitable for this use[4].

First, the creation time of quarks scales with the inverse mass of the quark. Due to their large mass, the heavy quarks are produced in quark-antiquark pairs before the QGP is created, as a result they experience the entire time of existence of the QGP.

The second factor that makes heavy quarks suitable as probes is the so-called *dead-cone effect*. Particles traversing a vacuum lose energy due to gluon-radiation. The dead-cone effect states that the gluon-radiation is suppressed for angles θ with $\theta < m/E$. Here m and E are respectively the mass and energy of the quark. This inverse mass dependence increases the chances of heavy quarks to survive the QGP, instead of losing so much energy that they decay while still inside the QGP.

Apart from gluon-radiation quarks can also lose energy inside the QGP due to collisions with other quarks and gluons. At the end of the QGP, all quarks form bound states inside hadrons again. Heavy quarks can be accessed by studying

the production of heavy mesons, like D and B mesons. These mesons cannot be measured directly, due to their short time of existence. Using the detectable final particles from their decay they can be reconstructed. The process of a beauty quark traversing the QGP, then binding with a light quark to form a B meson and (followed by) this meson decaying into lighter, detectable hadrons, is shown schematically in Figure 3[4].

Evidence of this energy-loss of heavy quarks is already provided by the substantial difference in the p_T distribution of heavy-flavour decay leptons, D mesons and non-prompt J/ψ in heavy-ion collisions compared to pp collisions. This modification can be described by the *Nuclear Modification Factor R_{AA}*. This variable is defined as the ratio between the yield of particles in nucleus-nucleus collisions divided by that of proton-proton collisions, scaled to take into account the difference of nuclei participating. If no nuclear effects appear, R_{AA} is unity. If quarks lose energy traversing the QGP, this leads to a suppression of hadron yields at $p_T > 3$ GeV/c, so that $0 < R_{AA} < 1$[7].
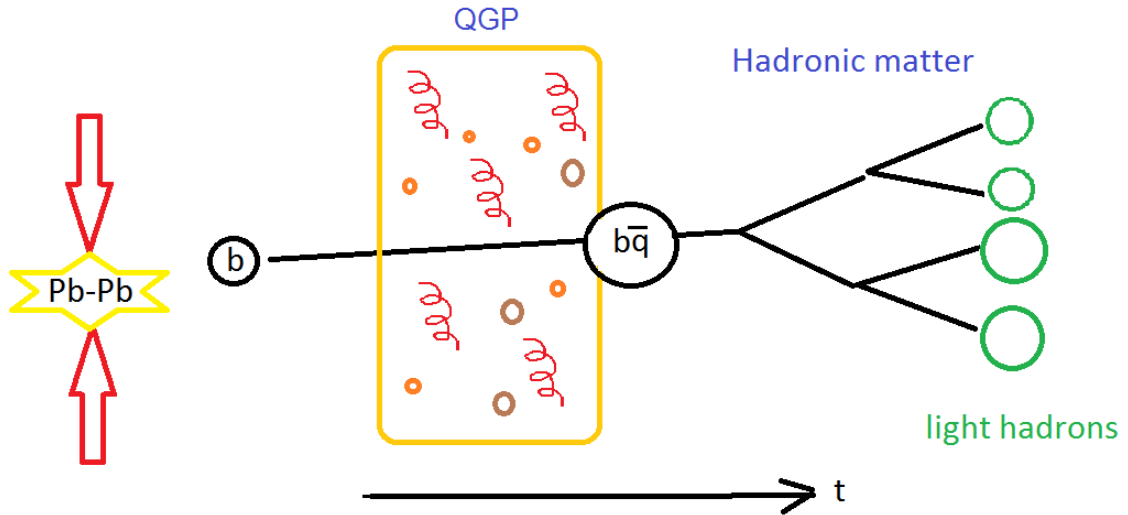

Figure 3 – A schematic view of using a beauty-quark as a probe to investigate the QGP generated in a lead-lead collision. $\bar{q}$ represents a light quark. The x-axis represents time.

Due to the high energy inside the QGP, there is a lower threshold for $s\bar{s}$ production. As a result, there is expected to be an abundance of strange quarks. This could effect the formation of strange mesons inside the QGP and is expected to enhance the R_{AA} of strange mesons with respect to their non-stange counterpart. There has already been looked for prove of this strangeness enhancement for D_s mesons coming from charm quarks, but the results were not sufficient to draw conclusions[7].

With the current particle accelerators and detectors, the reconstruction of B-

mesons has not been good enough to do this R_{AA} comparison. Due to a planned upgrade of the Large Hadron Collider and the ALICE detector (more on this in Section 2.1 and 2.2) it is now for the first time possible to even consider this.

To use top quarks, the heaviest quark flavour, as probes is not currently possible. They decay too fast to be detected. Even with the planned upgrade the resolution of the detector is too low to detect a particle decaying so fast after it was created[8].

As mentioned, the results of the heavy-quark meson yields have to be compared to pp results where the QGP is absent. These two results together enable the determination of the R_{AA}. This particularly difficult for particles including a beauty quark, since they are so rare in pp collisions[4].

1.4 Research question

In this thesis, the feasability of reconstructing the B_s^0 meson with the results of the ALICE detector pp collisions at 14 TeV after the upgrade is investigated. This reconstruction would provide a reference frame for measurements on this meson in Pb-Pb collisions.

The used method is a simulation study of the decay that is schematically shown in Figure 4. Since the B_s^0 and $\bar{B}_s^0$ can both decay through this decay channel, with B_s^0 in this thesis, will be referred to both the B_s^0 meson and its antiparticle $\bar{B}_s^0$. With D_s I refer to both the D_s^+ and the D_s^- particle. This is a fully hadronic decay, which means that all particles participating in the decay can be detected or reconstructed with the ALICE detector. This will be further explained in section 2.2.

1.5 Structure of this thesis

The contents of this thesis is organized as follows: In chapter 2.1 and 2.2 the setup of the ALICE experiment is found. In chapter 2.3 the setup of the Monte-Carlo simulations used for this thesis is explained. The results of the simulations are given in chapter 3. Chapter 4 contains the discussion. Chapter 5 presents the conclusion and outlook.
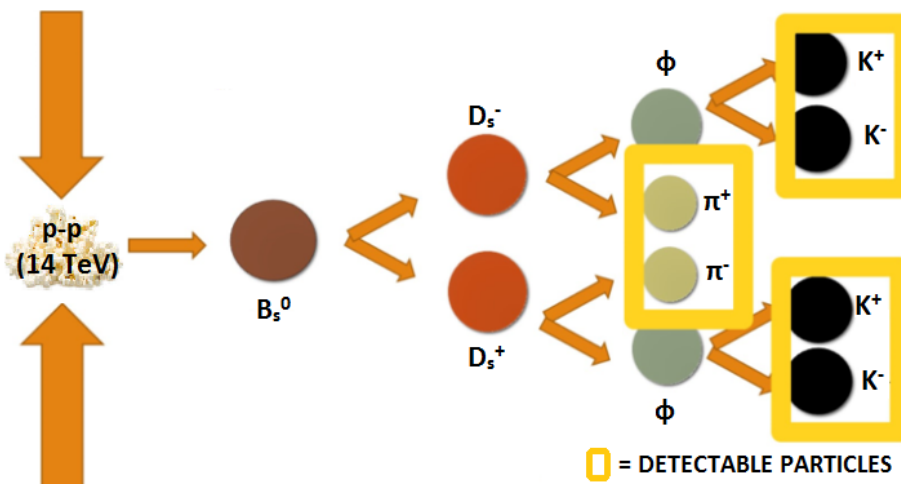
Figure 4 – A fully hadronic decay of the B_S^0 meson. This is the decay that is used for this thesis. The final particles that are detectable with the ALICE detector are surrounded by a yellow box. The other particles have a lifetime that is too short for the particles to be detected.

2 Experimental Setup

2.1 The Large Hadron Collider

The Large Hadron Collider (LHC) is the worlds largest and most powerful particle accelerator. It is located at Cern (Switzerland) and consists of a 27-kilometer ring that accelerates two beams of particles inside. To accelerate lead beams of particles and lead them in the right direction it uses superconducting magnets at a very low temperature. When the beams have gained a speed close to the speed of light they are made to collide. There are four locations on the ring where this collisions take place. This are the locations of four particle detectors: ATLAS, CMS, ALICE and LHCb. In Figure 5 the underground location of the LHC and its detectors are projected on a photograph of the area[9].

2.1.1 Upgrade of the LHC

During 2018-2019 the LHC will be upgraded. This upgrade will consist of installing improved technologies of the LHC. The goal of the upgrade is to improve the luminosity of the accelerator. This will lead to a higher collision energy of the experiment[10][11].

Figure 5 – The Large Hadron Collider. The yellow line marks the underground location of the LHC. The locations of the detectors are also marked. Figure adopted from [12].

2.2 The ALICE detector

One of the detectors at the LHC is the ALICE detector: A Large Ion Collider Experiment. The ALICE detector is designed to study the properties of strongly interacting matter, including the properties of the QGP. It uses proton-proton (p-p), proton-lead (p-Pb) and lead-lead (Pb-Pb) collisions from the LHC to obtain data. The energy generated by Pb-Pb collisions and measured by ALICE is high enough to create the QGP[10].

Figure 6 gives a schematic view of the ALICE detector. The detector consists of several parts for the tracking and identification of particles. Surrounding the detector is a big magnet that bends the tracks all charged particles with it's magnetic field. From the curvature of the tracks their momentum can be determined[13].

The detectors used for tracking and identifying hadrons are the Inner Tracking System (ITS), Time Projection Chamber (TPC), Transition Radiation Detector (TRD) and Time Of Flight detector (TOF). Other parts of the detector are used for detecting photons, electrons and muons and for triggering the detector when an interaction occurs. Together the ITS, TPC and TRC reconstruct the tracks of particles. The ITS, TPC and TOF detector are used to identify them[13].
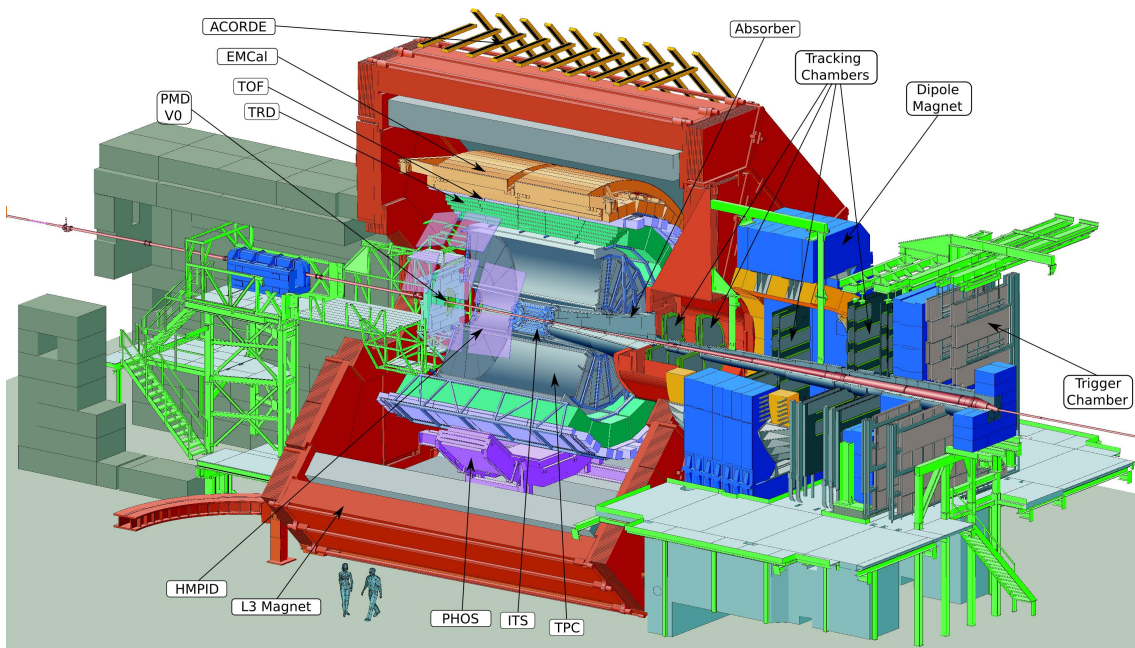

Figure 6 – The ALICE detector. Figure adopted from [14]

8

The detectors can determine the following properties that are relevant for this thesis:

- The pseudorapidity $|\eta|$: the angle of a particle perpendicular to the beam axis in GeV/c.

- The transverse momentum p_T: the momentum of a particle perpendicular to the beam axis.

- The distance between the interaction point and the decay point of a decayed particle in mm. This will be called the decay vertex in this thesis.

2.2.1   Inner Tracking System

At the center of the detector is the ITS. This part of the detector consists of high-resolution silicon detectors. The layer of silicon detectors closest to the beamline is at currently at a radius of 39 mm[10].

2.2.2   Time Projection Chamber

Around the ITS is the TPC. This is a gas-filled cylinder with an outer layer of read-out planes. When a charged particle passes through the TPC, it ionizes the gas. The electrons released by the ionizing of the gas drift towards the read-out planes. With the signals of the read-out planes it is possible to reconstruct a 3D track of the particle. The TPC also measures the energy loss $\frac{dE}{dx}$ of the tracked particles. This energy loss is used for the particle identification[15].

2.2.3   Time Of Flight detector

Around the TPC there is the TOF detector. This detector measures very precisely the time of every particle passing the detector. This time can be used to determine a particles velocity[13].

2.2.4   Upgrade of the ALICE detector

During the upgrade of the LHC in 2018-2019, the ALICE detector will also be upgraded. The ITS will be replaced by an improved ITS, that has a better resolution, lies closer to the beamline and a faster read-out time. It will then be able to read-out all interactions generated with the upgraded LHC. The other detectors will also be upgraded, improving their read-out capacity[10][15].

After the upgrade the expected number of events generated with pp collisions with an energy of 13 TeV is around $30 * 10^9$[16]. In the best case scenario the energy will be 14 TeV. In this thesis the best case scenario of 14 TeV is used.

2.2.5 Limitations

The limitations of the ALICE detector relevant for this thesis are:[10]

- Particles with a pseudorapidity $|\eta|$ larger than 0.9 cannot be detected.

- Particles with a transverse momentum p_T smaller than 0.1 GeV/c cannot be detected.

- The detector's precision in getting p_T is not perfect. The measured value of p_T can deviate from the real value. The size of this deviation depends on the momentum region in which the particle is and is larger for small p_T.

- The detector cannot track charge-less particles like neutrons and neutrinos

2.3 Simulation setup

2.3.1 PYTHIA

To simulate events used the program PYTHIA has been used (version 8.209). For the part where calculating the fraction of B_s^0 per event, minimum bias simulations were used, this means the settings are as close to reality as possible.

The setting used for minimum bias simulations is:

- HardQCD:all=on

For the parts where getting properties of rare particles, like the B_s^0 meson, forced settings have been used.

Each number represent a certain particle and these settings first switch of all decays of a certain particle and then only switch on the desired decay of this particle. Depending on the situation either all of these settings or only a part of them were switched on.

The settings used for the forced simulations are:

- HardQCD:hardbbbar=on

- 531:onMode = off

- 531:onIfMatch = 431 -431

- 431:onMode = off

- 431:onIfMatch = 333 211

- 431:onIfMatch = -333 211

- -431:onMode = off

- -431:onIfMatch = 333 -211

- -431:onIfMatch = -333 -211

- 333:onMode = off

- 333:onIfMatch = 321 -321

- -333:onMode = off

- -333:onIfMatch = 321 -321

2.3.2 ROOT

To process the information from the PYTHIA events and create the histograms that are part of the final results of my thesis the program ROOT has been used (version v5.34/30).

3 Results

3.1 Plots

For some results in this section only the D_s particles with detectable final particles were selected. By this is meant that all final particles of the decay ($K^+K^-\pi^+K^+K^-\pi^-$) have a pseudorapidity and transverse momentum within ALICE detection limits: $|\eta| < 0.9$ and $p_T > 0.1$ GeV/c.

The number of events generated for the figures and tables are listed in Table 1.

Figure/Table	Number of events
Figure 7	From Bs0: $1 * 10^9$ Not from Bs0: $33 * 10^9$
Figure 8, Figure 10	From Bs0: $1 * 10^9$ Not from Bs0: $50 * 10^9$
Figure 10	$58.6 * 10^9$
Figure 11, Figure 12, Figure 14	From Bs0: $58.6 * 10^9$ Not from Bs0: #Ds in event $>= 2$: $304 * 10^9$ Not from #Ds in event: all: pdbt
Table 4	$B_s^0 \rightarrow D_s^+ D_s^-$: $1.82 * 10^9$ $D_s \rightarrow \phi\pi$: $3.24 * 10^9$ $\phi \rightarrow K^+K^-$: $3.24 * 10^9$
Table 3	All final particles detectable: $7.1 * 10^9$ Number of B_s^0 expected per event: $16 * 10^9$

Table 1 – Number of events used for the figures and tables.

3.1.1 Pseudorapidity

In Figure 7, the pseudorapidity distributions of D_s particles from B_s and not from B_s are compared. Both distributions are normalized to 1.

In the upper plot, it is visible that the pseudorapidity of D_s particles from B_s^0 is distributed closer to zero than the pseudorapidity of D_s particles not from B_s^0. This is also visible in the peak in the lower plot of the ratio between the two pseudorapidity distributions at $\eta = 0$.

In Figure 8, the difference in pseudorapidity of D_s particles from the same B_s^0 is shown for different B_s^0 p_T bins. This is only for D_s particles with detectable final particles in a forced decay. For all p_T bins distribution is peaked at $\Delta\eta = 0$.

For higher p_T bins this peak becomes sharper, meaning the angle between the D_s particles from the decay $B_s^0 \to D_s^+ D_s^-$ becomes smaller.
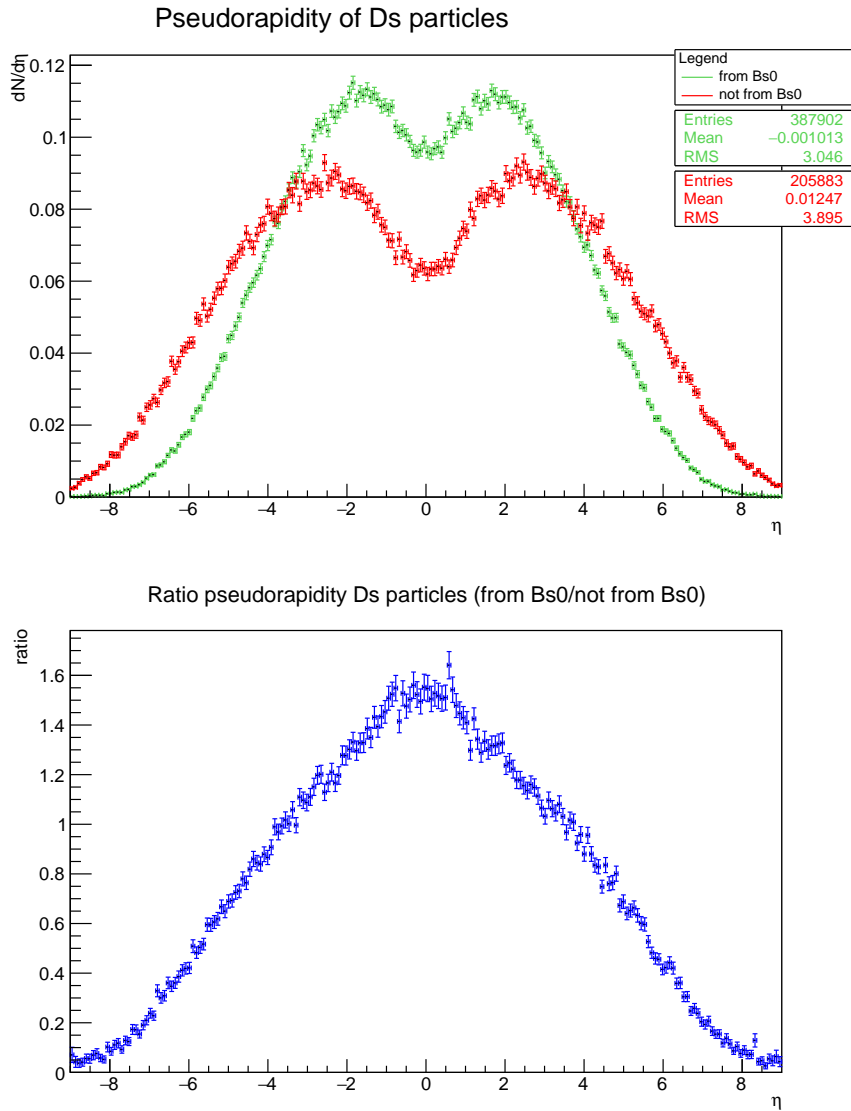

Figure 7 – Upper plot: Pseudorapidity η of D_s particles from B_s (forced simulation, green symbols) and not from B_s (minimum bias simulation, red symbols). Lower plot: The ratio between the two results.
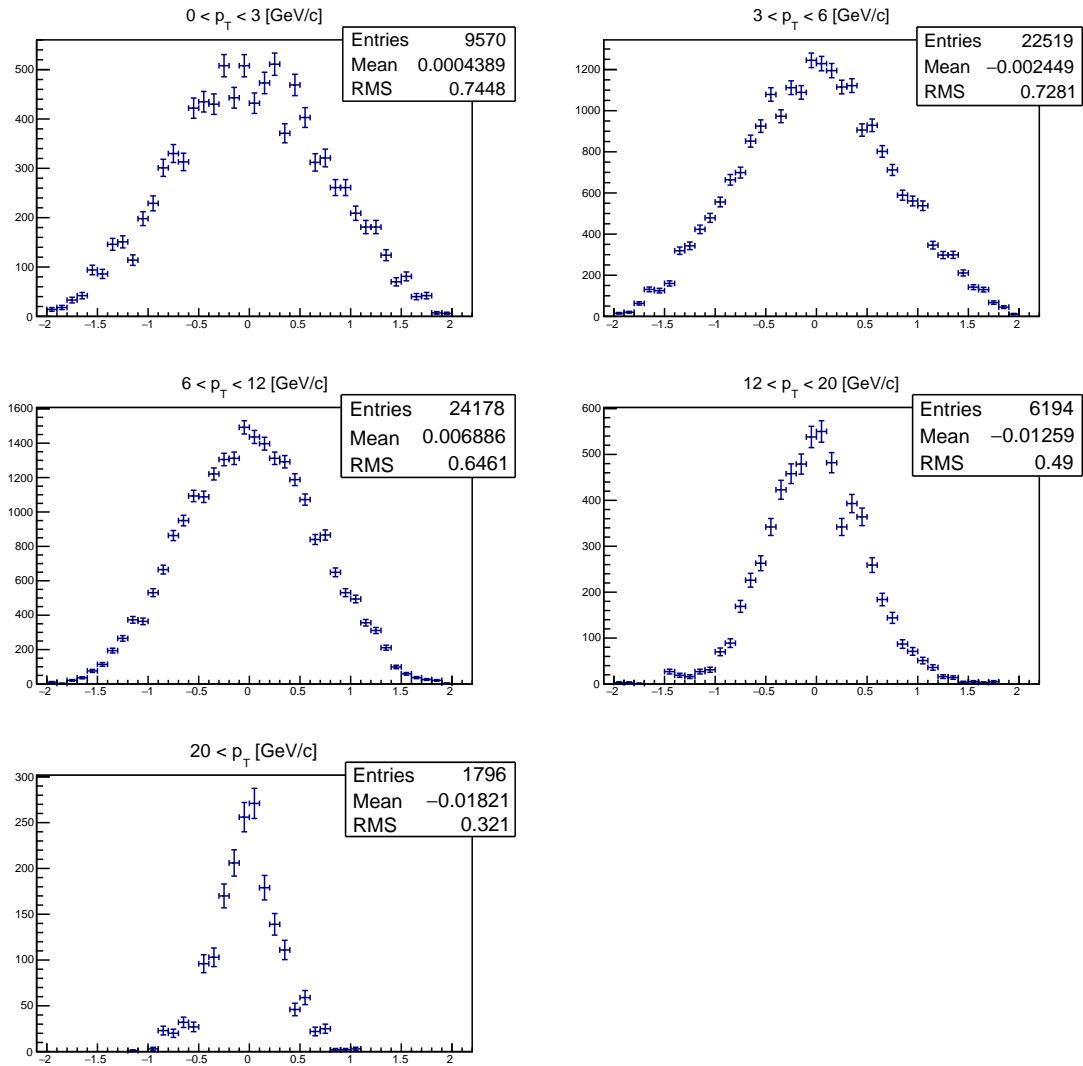
Figure 8 – Upper plot: Difference in pseudorapidity η of D_s particles from B_s for different p_T bins in a forced simulation with all final particles detectable.

3.1.2 Transverse momentum

In Figure 9, the transverse momentum distributions of all particles participating in the selected decay of the B_s^0 meson is shown. All distributions are normalized to an integral of 1. For all distributions a forced simulation is used. The average transverse momentum of B_s^0 highest. Then in declining order: D_s, ϕ, π and K.
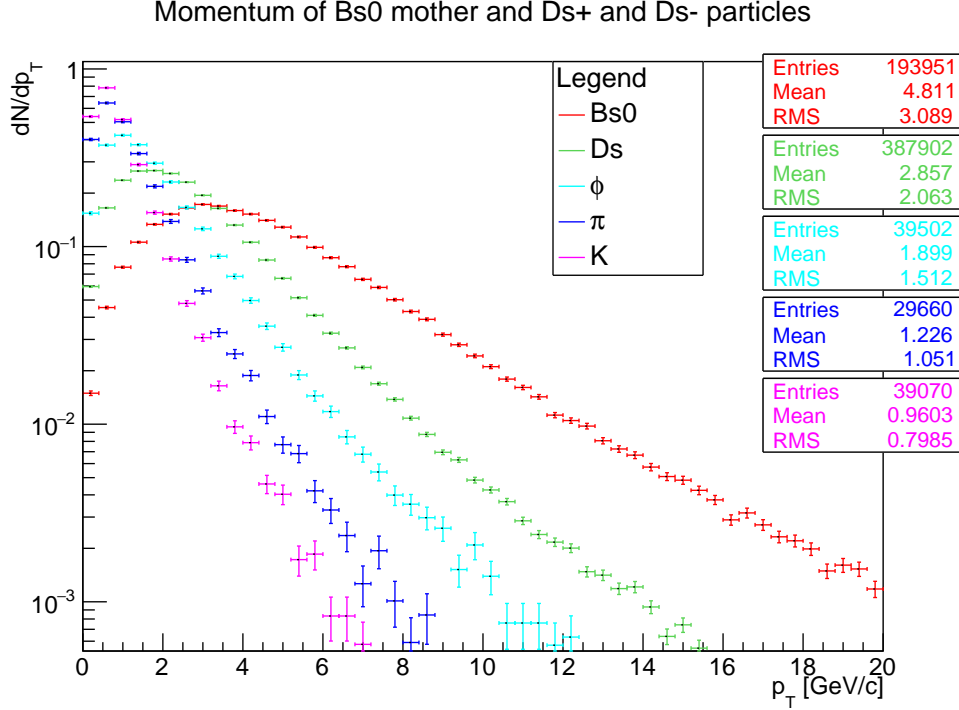

Figure 9 – Momentum distributions of all particles participating in the selected decay of B_s^0.

In Figure 10, the transverse momentum distributions of D_s particles from B_s^0 and not from B_s^0 are compared. Both are normalized to an integral of 1. The distribution of D_s from B_s^0 is forced, for the distribution for D_s not from B_s^0 the decay of the D_s particles is forced. The p_T distribution of D_s particles not from B_s^0 is closer to zero than the one from B_s^0. This is also visible in the increase of the ratio for higher p_T. For $p_T > 10$ GeV/c the number of entries for D_s not from B_s^0 is so small that most bins are empty.
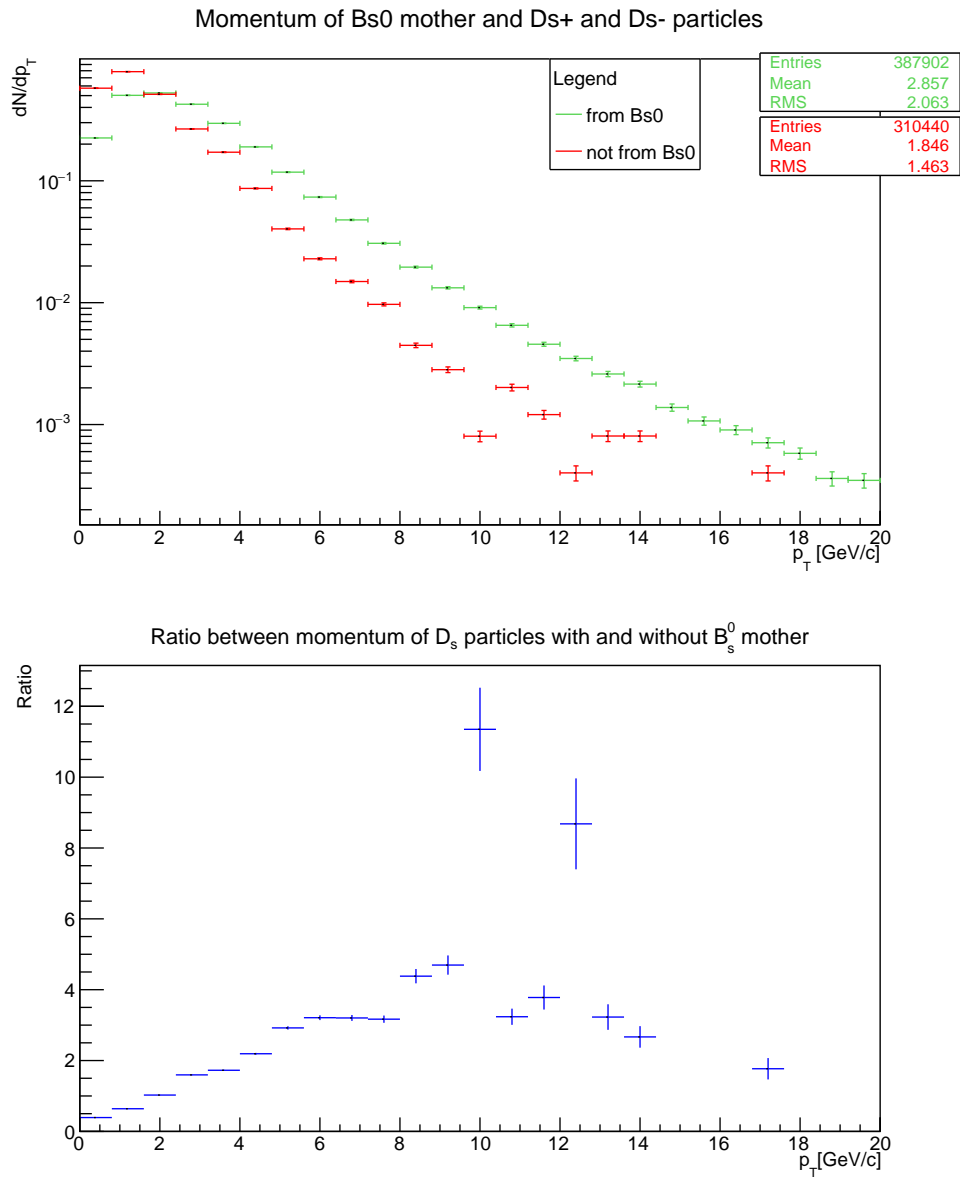
Figure 10 – Upper plot: Transverse momenta of D_s particles from B_s (forced) and not from B_s with all final particles detectable. Lower plot: The ratio between the two results. For $p_T > 10$ GeV/c there are no entries for some bins of the "not from B_s^0 distribution.

In Figure 11, the p_T distribution of D_s particles from B_s^0 is shown for different bins of B_s^0-p_T. For higher p_T bins the number D_s with high p_T is higher than for the lower p_T bins. This is also visible in the increasing mean value of the distributions shown in the lower right plot of Figure 11.
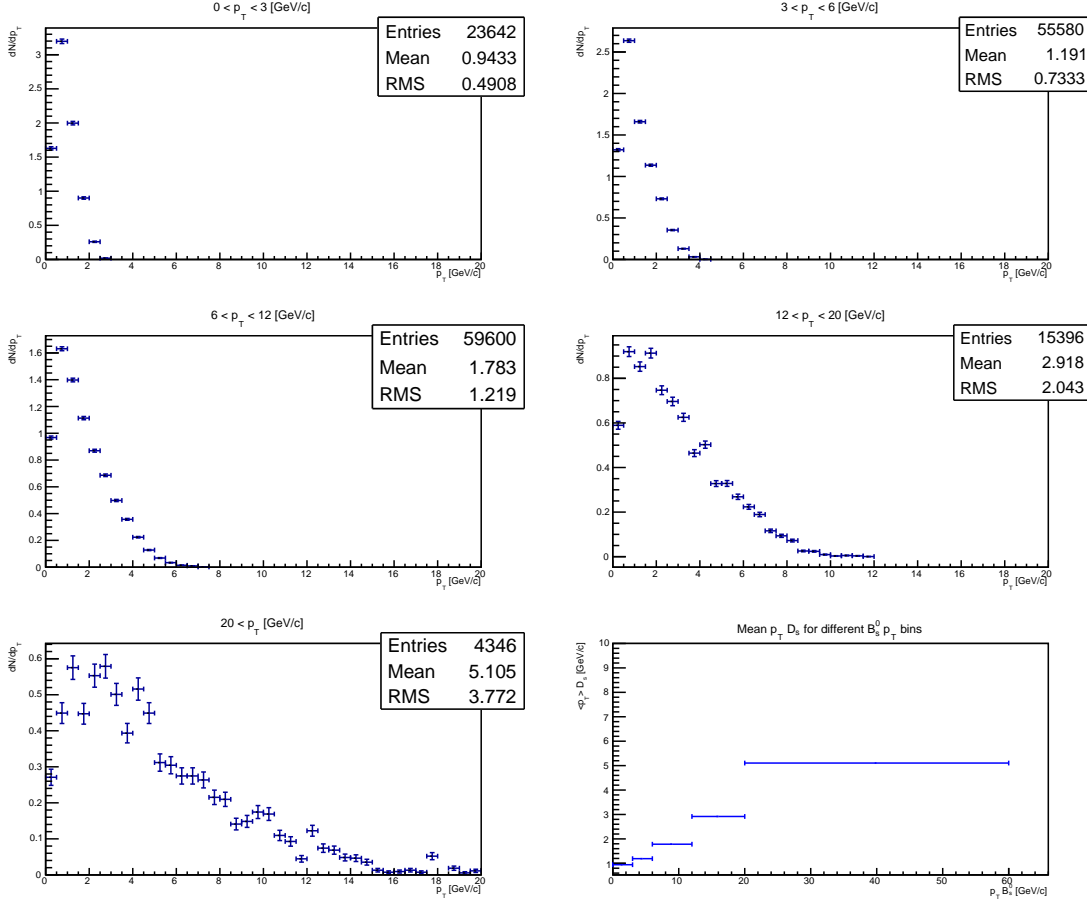

Figure 11 – Transverse momenta of D_s particles from B_s in bins of B_s^0 p_T with all final particles detectable. The plot on the lower right shows the mean values of the momentum-distributions for the different p_T bins.

3.1.3 Decay vertex

In Figure 12, the decay vertex distributions of D_s particles from B_s^0 and not from B_s^0 are shown, all normalized to an integral of 1. For the ones not from B_s^0 there is a distribution shown for all D_s and one for only the ones where two or more D_s are present in one event. Of the D_s not from B_s^0 a large part decays with a decay vertex $s < 0.01$ mm. The distribution for D_s from B_s^0 peaks around $s = 0.2$ mm. The ratio between the two distributions is highest at $0.5 < s < 2$.

In Figure 13, the purity of D_s from B_s^0 is shown. The purity is the ratio number of D_s from B_s^0 left for $s < $ some value x divided by the total number of D_s left. This ratio is shown for all D_s and for the case when only the D_s when two of more are present in one event. The purity increases rapidly from $s = 0$ to $s = 0.01$ and after that it continues to increase, but with decreasing slope. The purity for all D_s is lower than the purity compared to D_s when two of more are present in one event.

In Figure 14, the distribution of decay vertex is shown for different intervals of p_T of B_s^0. The two variants where the decay distance of D_s particles not from Bs^0 is shown, the different diagrams are filled with D_s particles of momentum matching the momenta of D_s particles coming from B_s^0 with p_T withing that bin. In figure 15 the mean values of these distributions are shown.

Below in Table 2 is a list given with matching momentum bins for B_s^0 and D_s^0 particles, based on Figure 11.

B_s^0 p_T	D_s p_T
0-3 GeV/c	0-1.5 GeV/c
3-6 GeV/c	1.5-3 GeV/c
6-12 GeV/c	3-5 GeV/c
12-20 GeV/c	5-9 GeV/c
20+ GeV/c	9+ GeV/c

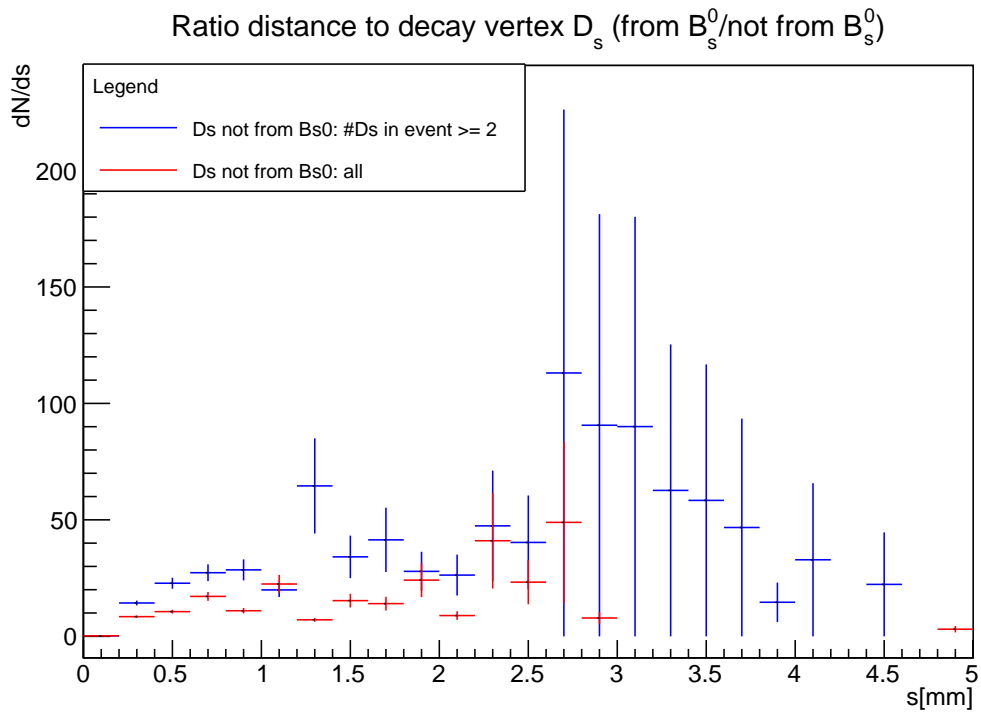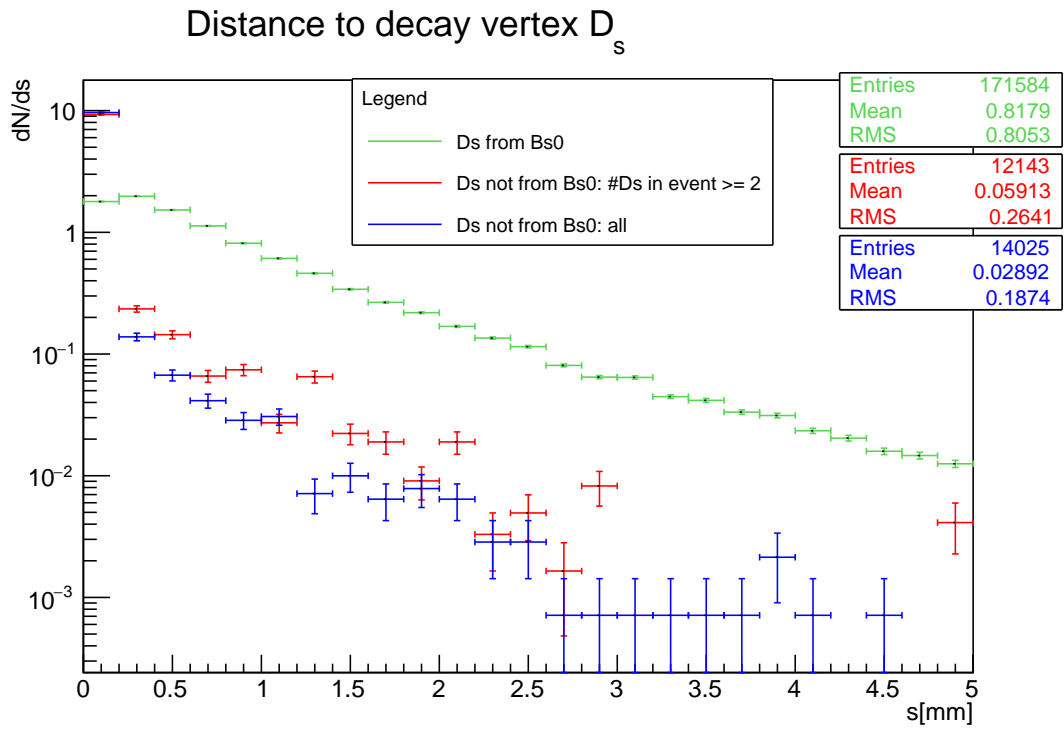**Table 2** – Matching D_s and B_s^0 p_T bins

Figure 12 – Upper plot: Distance to decay vertex of D_s particles from B_s and not from B_s with all final particles detectable. Lower plot: The ratio between the two results.
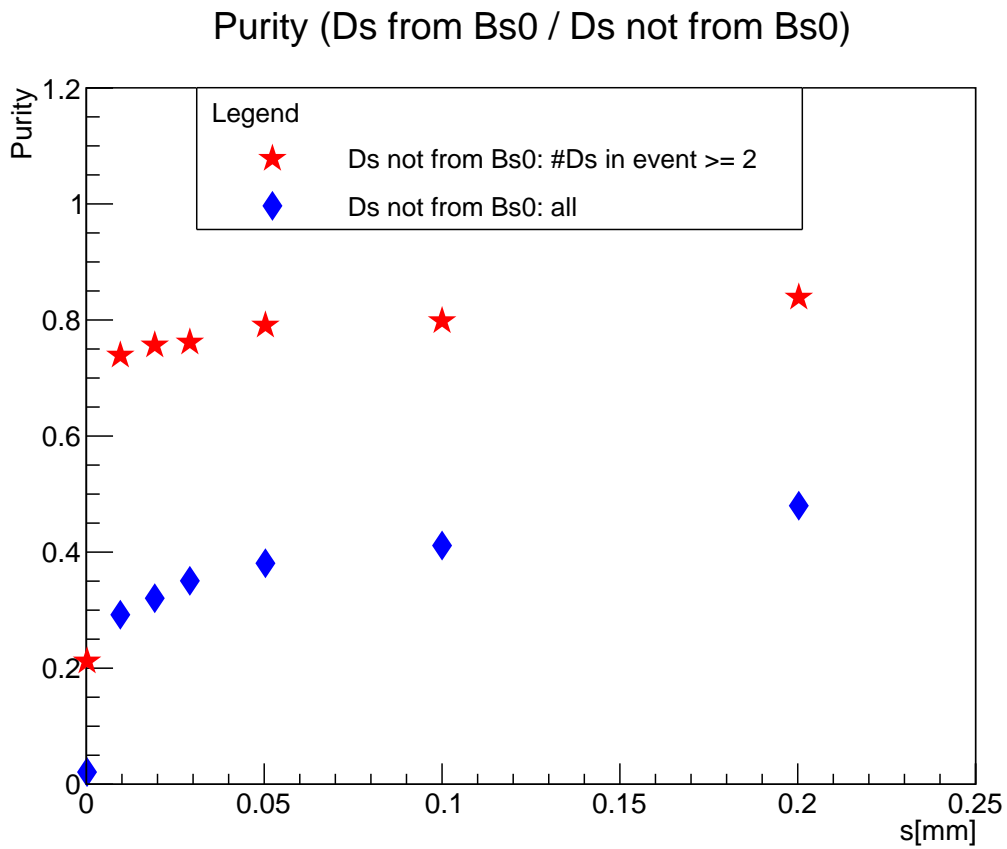
Figure 13 – Purity of D_s from B_s^0 plotted against the distance to the decay vertex of the cut.

Figure 14 – Distance to decay vertex of D_s from B_s^0 and not from B_s^0 plotted for different p_T bins with all final particles detectable. On the lower right plot the mean values of the distributions per p_T-bin are plotted.

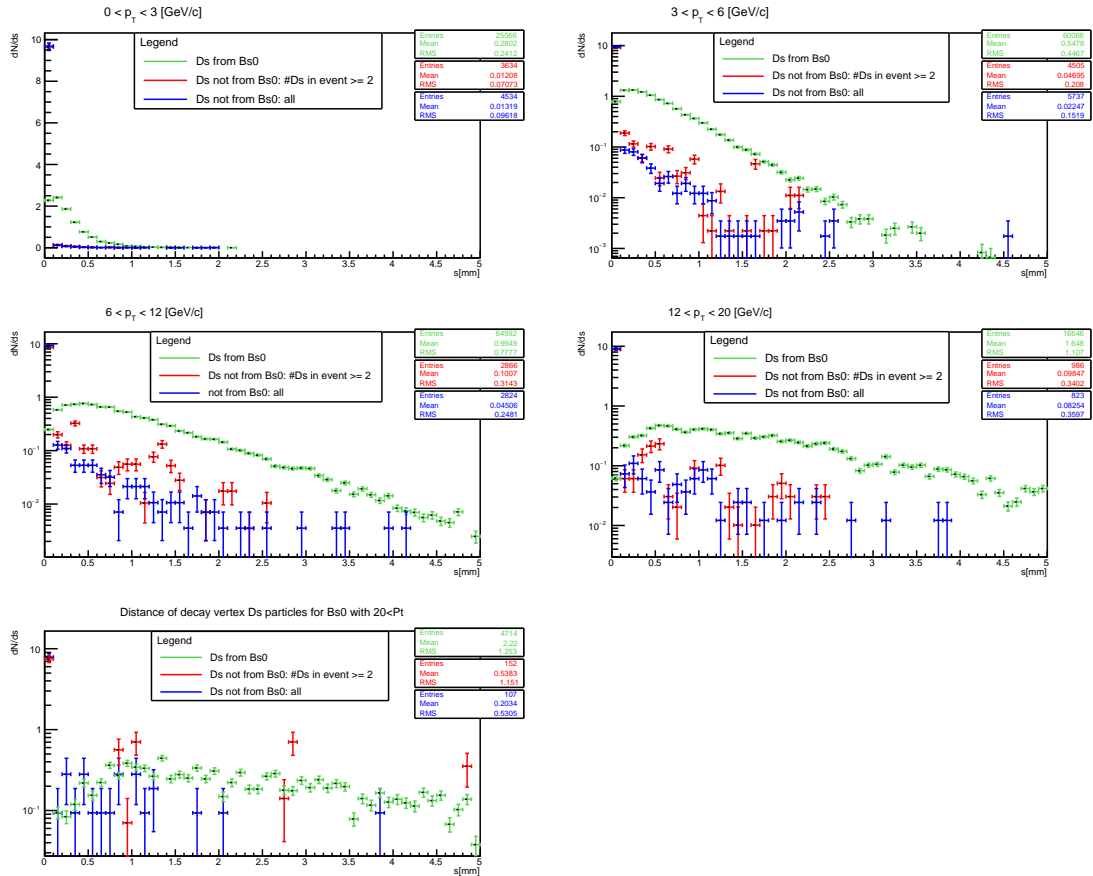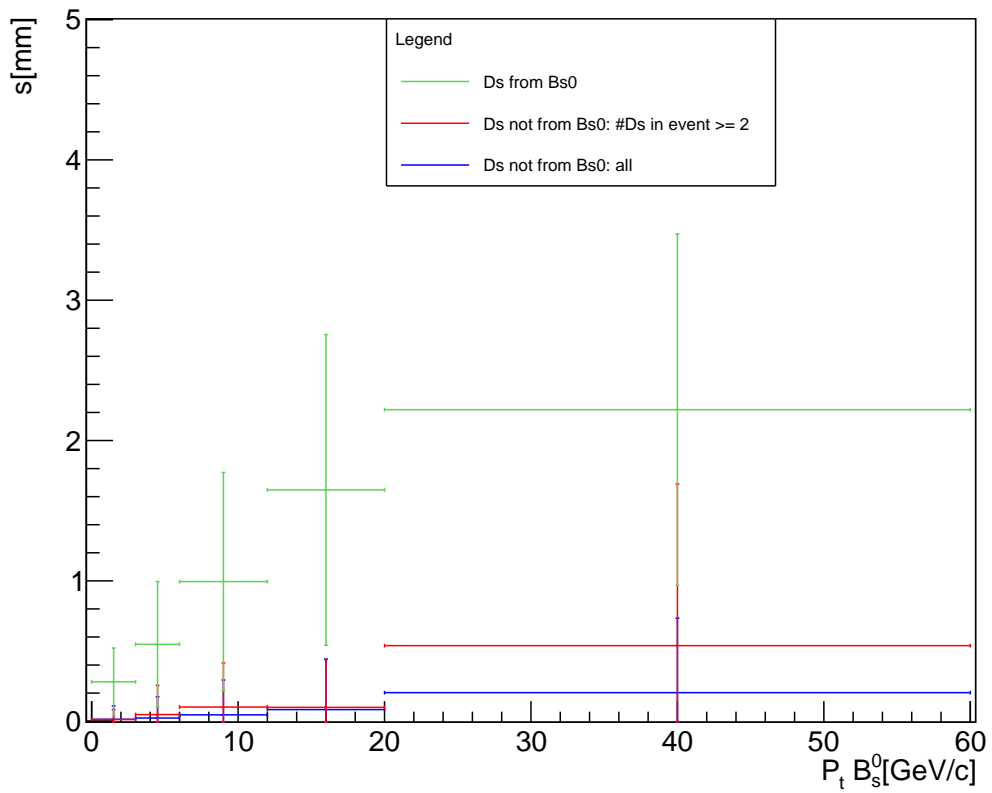**Figure 15** – The mean values of the distributions per p_T-bin of the distance to decay vertex of D_s from B_s^0 and not from B_s^0 plotted for different p_T bins with all final particles detectable.

3.2 Estimate for a possible measurement

In Table 3 the fractions of each decay from the chosen decay ($B_s^0 \rightarrow D_s^+ D_s^- \rightarrow \phi\pi^+\phi\pi^- \rightarrow K^+K^-\phi^+K^+K^-\phi^-$) are given. At the bottom of the table the total fraction of the decay is calculated.

In Table 4 the final calculation of the fraction of detectable decays with the limitations of the ALICE detector and including the fraction of expected B_s^0 mesons per event is shown. Note that the decay fractions of D_s and ϕ both occur twice in the calculation of the fraction of detectable decay per event.

The number of events on which this calculations are based are listed in Table 1.

Decay	Fraction
$B_s^0 \rightarrow D_s^+ D_s^-$	$8.7 * 10^{-3}$
$D_s \rightarrow \phi\pi$	$4.5 * 10^{-2}$
$\phi \rightarrow K^+K^-$	$4.9 * 10^{-1}$

Table 3 – Decay fractions of $B_s^0 \rightarrow D_s^+ D_s^- \rightarrow \phi\pi^+\phi\pi^- \rightarrow K^+K^-\phi^+K^+K^-\phi^-$.

Decay	Fraction
$|\eta| < 0.9$ and $p_T > 0.1$ GeV/c for all final particles	$6.25 * 10^{-2}$
Number of B_s^0 expected per event	$1.72 * 10^{-4}$
Fraction of detectable decay per event	$4.39 * 10^{-11}$
Number of expected detected decays with the upgraded ALICE detector	1

Table 4 – Detector expectation fractions and values.

4 Discussion

The main limitation of the reconstruction of the B_s^0 particle is the number of decays detectable. The total fraction of detectable B_s^0 with the ALICE detector is 0.04 per billion. The expected number of events is around 30 billion, which would lead to an expected number of detected events of 1. This is not enough for the reconstruction.

There are other findings about this decay that might be useful for further studies:

It is found that the pseudorapidity-distribution of D_s particles from B_s^0 is closer to zero than the one not from B_s^0 and the drop at zero is shallower. One of the limitations of the ALICE detector is that it can only measure particles with $|\eta| < 0.9$. This improves the chances of the ALICE detector being able to detect the D_s particles from B_s^0 compared to the ones that are not from B_s^0. There are still a lot of particles lost that are outside this η region.

It is shown that the difference in the two D_s particles from the decay is distributed in a peak around zero. For higher momentum this peak becomes narrower. This would improve the chance at detecting high-momentum B_s^0, because then the chance at all final particles being within $|\eta|$ range is bigger.

The momentum distributions of all particles participating in the decay of the B_s^0 meson are shown. These distributions do not give any surprising results.

The momentum of D_s particles from B_s^0 is compared to the ones not from B_s^0. The ratio of these two distributions rises for higher momentum. The chances detecting D_s from B_s^0 thus improve at higher momentum. A downside of cutting at high momentum is that there will be lost a lot of particles that are coming from B_s^0 too. For $p_T < 3$ the number of particles not from B_s^0 is higher than the number of particles fron B_s^0. For $p_T > 3$ there are more from B_s^0.

The momentum of D_s particles from different B_s^0 p_T bins is compared. The average momentum of the D_s particle is higher for D_s coming from higher p_T. This is a would be expected, since B_s^0 with high p_T have more energy to pass on to the D_s particles.

The distance from the collision point to the decay vertex of the D_s particle from B_s^0, not from B_s^0 and with two or more D_s particles in the same event with opposite charge and all D_s particles not from B_s^0 are compared. The first distribution peaks at 0.2 mm and than slowly decreases. Between the latter two there does not seem to be significant difference. They both have a very high peek between 0 and 0.01 mm and than quickly decrease towards 0. The ratios both rise rapidly between 0 and 1.5 mm. After this, they decrease again, but they continue to be above 1.

The purity of D_s particles from B_s^0 is compared to the total number of D_s parti-

cles in a sample for the case were only the ones with two or more D_s particles with opposite charge are in the same event and for all D_s particles when all particles below decay vertex s are cut out. Both purity plots rise very fast between 0 and 0.01 mm. After that the slope decreases and at 0.2 mm it is almost flat. The one where all D_s particles are taken into account is a bit steeper, but not enough no compensate for the lower purity it has for the no-cut case shown at $s = 0$.

The mean decay vertex divided in different B_s^0 p_T bins for all three distributions rise as a function of p_T. This is what would be expected. The mean value of D_s from B_s^0 rises with a higher slope than both distributions for D_s not from B_s^0. The method of combining a D_s momentum with a B_s^0 momentum in order to be able to divide the D_s not from B_s^0 in momentum bins was not very evident, so this comparison is not perfect.

To reconstruct B_s^0 mesons decaying into $D_s^+ D_s^-$ cutting out D_s particles with a decay vertex < 0.01 would improve the purity of the sample significantly.

What has not been taken into account in this thesis is the efficiency of the detector, which is not perfect. There is also a deviation in the measurement of the particle momentum. The average magnitude of this efficiency and deviation depends on the momentum of the particle[10].

Since the efficiency in pseudorapidity of the ALICE detector, the variation due to small errors in p_T measurement and possible cuts are not yet taken into account in this result, the actual expectation value would be even lower.

5 Conclusion

Based on the previous section it is possible to conclude that for the detection of B_s^0 mesons it would be a smart step to cut out D_s particles with low momentum (at least all particles with $p_T < 3\text{GeV/c}$) and with small decay vertex (at least all particles with $s < 0.01$ mm).

However, the estimate of only 1 decay to be detected leads to the conclusion that it is very unlikely that the reconstruction of B_s^0 through this decay will succeed. This is due to the low frequency of the chosen decay happening combined with the imperfect detecting efficiency of the ALICE.

An alternative for studying the beauty quark through full hadronic reconstruction of the B_s^0 meson might be using a semi-leptonic decay of one of the D_s particles coming from B_s^0, including an electron. This is a decay consisting of one lepton and it's corresponding neutrino and at least one hadron. This way there could be triggered on a high-energy electron, which would improve the number of particles available for reconstruction. An example of a semi-leptonic decay of the D_s meson that could be used is $D_s^+ \rightarrow \phi e^- \nu_e \rightarrow K^+ K^- e^- \nu_e$[17]. Research into the feasibility of this sort of reconstruction is still ongoing[18].

Another option could be to use high-energy electron triggering, but continue to use the full hadronic decay. The high-energy electron would then have to come from the other beauty quark of the $b\bar{b}$ pair.

For both this options the cuts in decay vertex and momentum of the D_s particles could still be used.

References

[1] Martin, B. R. *Nuclear and Particle Physics*. John Wiley & Sons Ltd, The Atrium, Southern Gate, Chichester, West Sussex PO19 8SQ, England, 2006.

[2] Greene, B. How the higgs boson was found. *Smithsonian Magazine*, July 2013, 2013.

[3] The University of Tokyo. Countdown underway for higgs boson discovery, 2012. Accessed through `http://www.u-tokyo.ac.jp/en/utokyo-research/feature-stories/atlas2012/` at 17/12/2016.

[4] Grelli, A. Heavy-quark production in high-energy heavy-ion collisions. Lecture, April 2014.

[5] Satz, H. The Quark-Gluon Plasma: A Short Introduction. *Nucl. Phys.*, A862-863:4–12, 2011.

[6] Iancu, E. QCD in heavy ion collisions. In *Proceedings, 2011 European School of High-Energy Physics (ESHEP 2011): Cheile Gradistei, Romania, September 7-20, 2011*, pages 197–266, 2014.

[7] The ALICE collaboration, Adamov D. Adam, J., and et al. Measurement of ds+ production and nuclear modification factor in pb-pb collisions at $snn = 2.76$ TeV. *Journal of High Energy Physics*, 2016(3):82, 2016.

[8] Nakamura, K. and Particle Data Group. Review of particle physics. *Journal of Physics G Nuclear Physics*, 37(075021), July 2010.

[9] Cern. The Large Hadron Collider, 2017. Accessed through `https://home.cern/topics/large-hadron-collider` at 12/10/2016.

[10] Abelev, B. and others. Technical Design Report for the Upgrade of the ALICE Inner Tracking System. *J. Phys.*, G41:087002, 2014.

[11] Cern. The HL-LHC Project. Accessed through `http://hilumilhc.web.cern.ch/` at 12/17/2016.

[12] Cern. Building the HL-LHC with the Industry. Accessed through `https://project-hl-lhc-industry.web.cern.ch` at 12/17/2016.

[13] ALICE collaboration. Detectors of the ALICE experiment, 2008. Accessed through `http://aliceinfo.cern.ch/Public/en/Chapter2/Page3-subdetectors-en.html` at 12/10/2016.

[14] Skjerdal, K. Photoproduction of ρ^0 in ultra–peripheral nuclear collisions at ALICE. *J. Phys. Conf. Ser.*, 455:012010, 2013.

[15] ALICE collaboration. The ALICE Time Projection Chamber (TPC), 2008. Accessed through `http://aliceinfo.cern.ch/Public/en/Chapter2/Chap2_TPC.html` at 12/17/2016.

[16] Grelli, A. Personal correspondence.

[17] Olive, K. A. and others. Review of Particle Physics. *Chin. Phys.*, C38:090001, 2014.

[18] Institute of Subatomic Physics Utrecht Heavy Flavour Group. Group meeting, December 15 2016.